ACS Chemical Neuroscience

pubs.acs.org/chemneuro

Research Article

Identification of Novel Regulators of Zalcitabine-Induced Neuropathic Pain

Antón L. Martínez,[⊥] José Brea,[⊥] Eduardo Domínguez, María J. Varela, Marta Cimadevila, Catarina Allegue, Raquel Cruz, Xavier Monroy, Manuel Merlos, Javier Burgueño,* Ángel Carracedo, and María I. Loza*

Cite This: *ACS Chem. Neurosci.* 2021, 12, 2619–2628

Read Online

ACCESS | Metrics & More | Article Recommendations | Supporting Information

ABSTRACT: Neuropathic pain is one of the foremost adverse effects that worsens quality of life for patients undergoing an antiretroviral treatment. Currently, there are no effective analgesics for relieving it; thus, there is an urgent need to develop novel treatments for neuropathic pain. Previously, we described and validated F11 cells as a model of DRG (dorsal root ganglia) neurons. In the current work, we employed F11 cells to identify regulators of antiretroviral-induced neuropathic pain combining functional and transcriptomic analysis. The antiretroviral zalcitabine (ddC) increased the excitability of differentiated F11 cells associated with calcium signaling without morphological changes in the neuronal phenotype, mimicking the observed increase of painful signaling in patients suffering from antiretroviral-induced neuropathic pain. Employing RNA sequencing, we observed that zalcitabine treatment upregulated genes related with oxidative stress and calcium homeostasis. The functional impact of the transcriptomic changes was explored, finding that the exposure to zalcitabine significantly increased intracellular oxidative stress and reduced store-operated calcium entry (SOCE). Because the functional and transcriptomic evidence points toward fundamental changes in calcium signaling and oxidative stress upon zalcitabine exposure, we identified that NAD(P)H quinone dehydrogenase and the sarcoplasmic/endoplasmic reticulum calcium ATPase 3 were involved in zalcitabine-induced hyperexcitability of F11 cells. Overexpression of those genes increases the calcium-elicited hyperexcitability response and reduces SOCE, as well as increases intracellular ROS levels. These data do not only mimic the effects of zalcitabine but also highlight the relevance of oxidative stress and of calcium-mediated signaling in antiretroviral-induced hyperexcitability of sensory neurons, shedding light on new therapeutic targets for antiviral-induced neuropathic pain.

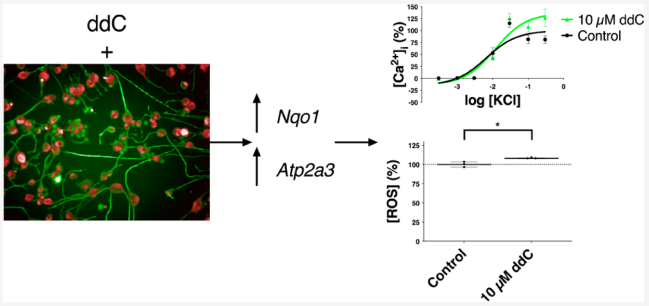

KEYWORDS: *Neuropathic pain, antiretrovirals, hyperexcitability, calcium transients, transcriptomic assays, adverse effects*

INTRODUCTION

Neuropathic pain is caused by injuries affecting either the central or the peripheral nervous system. It includes a wide range of pain processing alterations, including spontaneous pain generated by nonpainful stimuli (allodynia) or an exaggerated response to painful stimuli (hyperalgesia). Many etiologies, including diabetes, alcoholism, genetic diseases, metabolopathies, or infections, have been implicated in the pathogenesis of this syndrome.[1,2] One of the major causes of neuropathic pain is the side effects of drugs causing toxicity on peripheral sensory neurons.[3] This is the case of antiretroviral therapy with zalcitabine (ddC), a nucleoside analogue inhibitor of human immunodeficiency virus (HIV) reverse transcriptase, employed in the treatment of patients with HIV infection and related with the induction of neuropathic pain.[4]

One of the reasons why the alleviation of neuropathic pain is still an unmet clinical need is the underlying complexity of pain transmission and processing, which makes the identification of novel targets and analgesic drugs very challenging.[5] Dorsal root ganglia (DRG) neurons are responsible for transmitting pain signals from the periphery to the spinal cord. Primary DRG neurons would represent a perfect model for studying those disturbances affecting pain transmission through DRG neurons; however, the use of primary neurons in drug screening has several very significant drawbacks, such as the need to use animals for testing or labor-intensive isolation procedures.[6] Previously, we described a novel *in vitro* phenotypic assay in the hybrid mouse neuroblastoma and rat DRG neuron F11 cell line as an artificial translational model to overcome these drawbacks.[7] F11 cells acquire phenotypic

Received: March 8, 2021
Accepted: May 25, 2021
Published: June 29, 2021

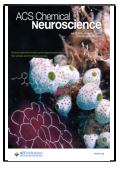

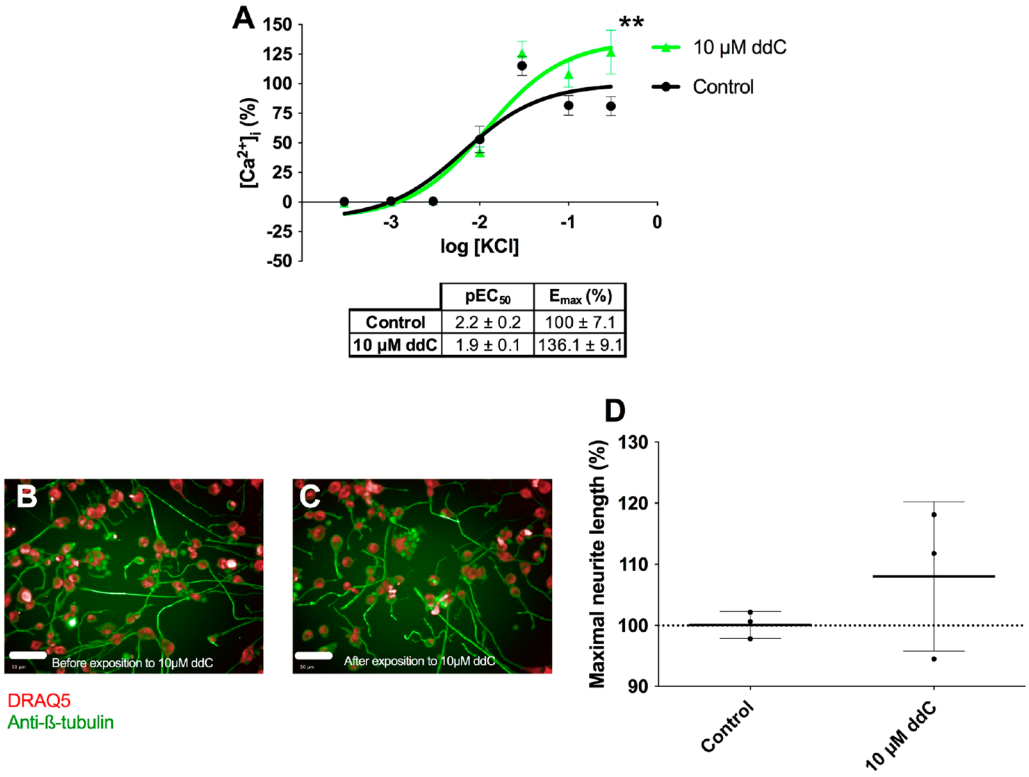

	pEC_{50}	E_{max} (%)
Control	2.2 ± 0.2	100 ± 7.1
10 μM ddC	1.9 ± 0.1	136.1 ± 9.1

Figure 1. Antiretroviral drug zalcitabine induces an increase in the intracellular concentration of calcium in response to KCl in differentiated F11 cells without changes in neurite length. (A) Increase in the intracellular concentration of Ca^{2+} elicited by KCl in differentiated F11 neurons exposed to 10 μM zalcitabine (ddC) during differentiation compared to control differentiated F11 cells. Values shown are means ± SD of four assays (n = 4) with triplicate measurements. ** $p < 0.01$ (extra sum-of-squares F test). Representative microphotographs of (B) control differentiated F11 cells stained against β-tubulin and in (C) differentiated F11 cells exposed to zalcitabine (ddC) during differentiation and (D) maximal neurite length before and after exposure to zalcitabine (ddC). Photographs are representative of three assays (n = 3) with 16 replicates per condition. Scale bar = 50 μm. Values shown for part D are means ± SD of three assays (n = 3) with 16 replicates per measurement.

features of DRG neurons after a differentiation process elicited by an increase in intracellular cAMP.[8,9] We employed F11 cells to identify new analgesics for neuropathic pain by quantifying the neuron excitability and demonstrated its utility to find novel drugs protecting against inflammatory mediators.[7] A transcriptomic study of this cell line in comparison to primary DRG cells was previously performed by Yin et al. in 2016,[10] finding that F11 cells express molecular markers present in primary DRGs and also receptors and ion channels relevant for nociceptive signaling.

Thus, our working hypothesis is that treating differentiated F11 cells with zalcitabine could lead to the identification of the mechanisms of zalcitabine-induced neuropathic pain. Therefore, we aim to deconvolute the effect of zalcitabine on differentiated F11 cells, employing a combination of functional and genomic assays.

RESULTS AND DISCUSSION

The major finding of this work was the identification of oxidative stress and calcium signaling as two mechanisms involved in zalcitabine-induced damage in an immortalized DRG neuronal cell line. We employed a combination of functional and transcriptomic approaches to identify two proteins involved in differentiated F11 cell hyperexcitability induced by zalcitabine.

One of the most prevalent adverse effects related to antiretrovirals is neuropathic pain, which is induced by different types of damage in peripheral neurons leading to hypersensitivity.[11] In our work, we aimed to deconvolute the mechanism of this harmful effect, by employing a combination of neuronal functional assays and transcriptomics in an immortalized sensory neuronal cell line. Thus, we exposed differentiating F11 cells to zalcitabine, an antiviral that has been related to the induction of neuropathic pain as an adverse effect.[12]

We observed, as previously described,[8] that about 50% of all F11 cells acquire phenotypic features of DRG neurons after differentiation. This is due to the nature of F11 cells as a hybridoma between DRG neurons and neuroblastoma cells. Exposure to zalcitabine during differentiation induced a significant increase in the entrance of calcium in response to KCl in differentiated F11 cells at an 80% of confluence, with a 36% increase in the maximal intracellular concentration of calcium ($p < 0.01$, extra sum-of-squares F test) (Figure 1A) but without significant changes in the EC_{50} of KCl. The observed increase in the amount of intracellular calcium concentration is consistent with the fact that calcium is implicated in the transmission of painful signals across DRG neurons[13] and with aberrant calcium levels in DRG neurons, which have been implicated in the pathogenesis of antiretroviral-elicited neuropathic pain.[14] This increase in the intracellular concentration of calcium was not accompanied by phenotypic changes in morphology (Figure 1B,C), neurite length (p = 0.2, Student's t test) (Figure 1D), nor connections in neurons compared to control differentiated F11 cells (Figure S1), denoting that, despite changes in the response of cells, morphology and

https://doi.org/10.1021/acschemneuro.1c00129
ACS Chem. Neurosci. 2021, 12, 2619−2628

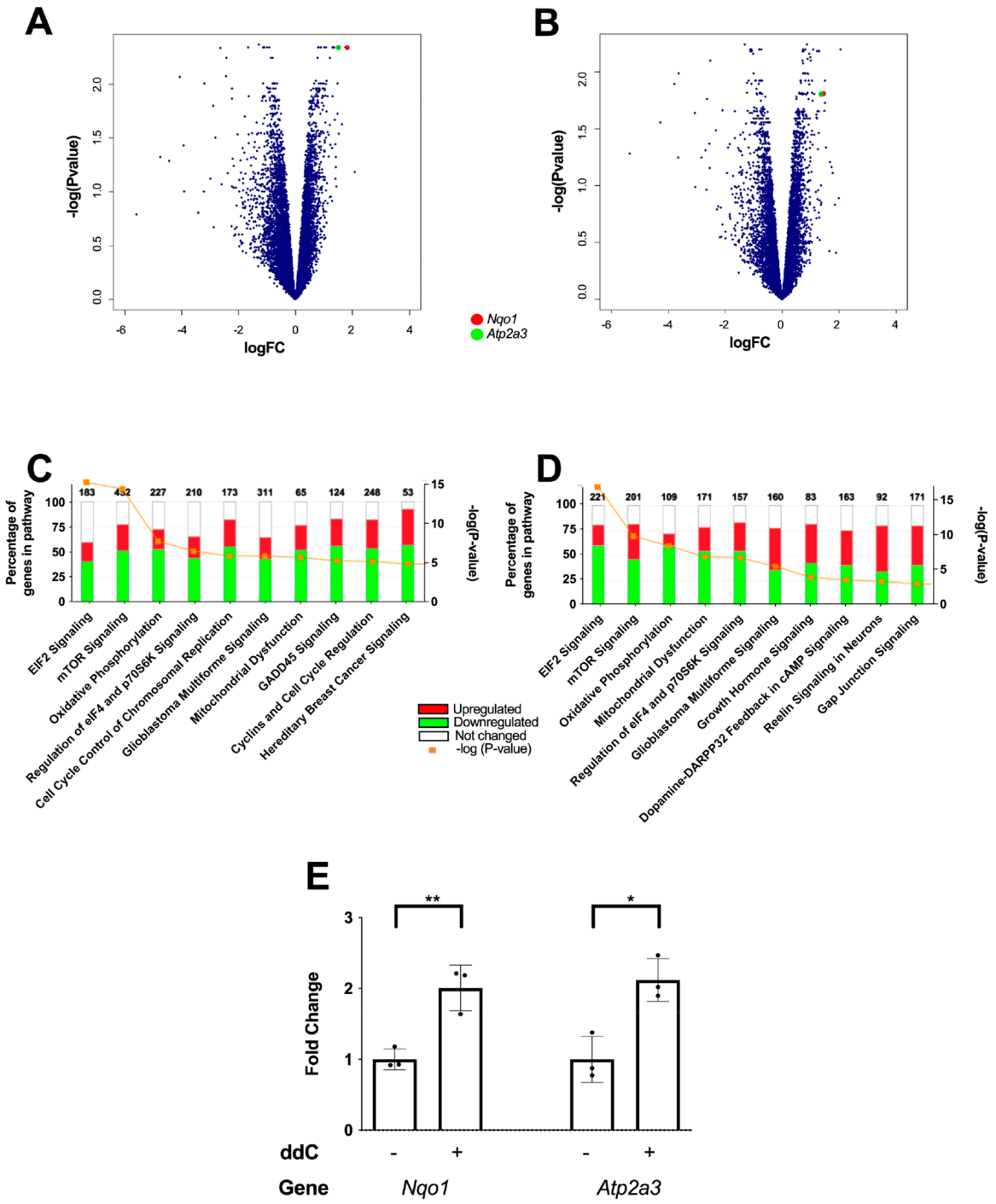

Figure 2. Exposure of differentiating F11 neurons to zalcitabine enhances the transcription of genes related with oxidative stress and calcium signaling. Volcano plot depicting the change in the expression of (A) mouse and (B) rat genes in F11 cells exposed to 10 μM zalcitabine during differentiation. Points are the mean of the values obtained with three RNaseq experiments performed with different samples. Changes observed in genes belonging to (C) mouse and (D) rat signaling pathways in differentiated F11 cells exposed to zalcitabine (ddC) during differentiation. (E) Comparative quantitation of the expression of *Nqo1* and *Atp2a3* genes in control differentiated F11 cells and in F11 cells exposed to 10 μM zalcitabine during differentiation employing RT-qPCR. Values shown are means ± SD of three assays (n = 3) with three replicates per measurement. ** $p < 0.01$; * $p < 0.05$ (Student's t test).

neuronal connections are preserved. This finding contrasts with the fact that the antiviral rilpivirine induced neurite shortening in differentiated F11 cells.[15] This difference may be explained by the fact that rilpivirine and zalcitabine present different chemical structures: Whereas rilpivirine is a non-nucleoside analogue reverse-transcriptase inhibitor, zalcitabine is a nucleoside-analogue reverse-transcriptase inhibitor.[16] Interestingly, it was previously described that, in iPSC derived cells, non-nucleoside analogue reverse-transcriptase inhibitors like rilpivirine induced neurite retraction, whereas nucleoside-analogue inhibitors like tenofovir or abacavir did not.[17]

In order to investigate which genes are involved in the increase of excitability of differentiated F11 cells after exposure to zalcitabine during differentiation, we compared the

https://doi.org/10.1021/acschemneuro.1c00129
ACS Chem. Neurosci. 2021, 12, 2619−2628

transcriptome of untreated differentiated F11 cells and of differentiated F11 cells exposed to the antiretroviral during differentiation. Zalcitabine elicited changes in the expression of 13 859 mouse genes (Figure 2A) and 11 270 rat genes (Figure 2B). We focused the scope of our study on the expression of genes involved in the defense against cellular damage. In particular, we observed an increase in the transcription of pathways and genes related to the defense against intracellular ROS (such as *Nqo1*) and to the regulation of intracellular calcium concentrations (such as *Atp2a3*) (Table 1). This finding is in agreement with the variations detected in the metabolic pathways, in which we observed that zalcitabine induces a repression in those genes that encode proteins related with obtaining energy from reducing agents like oxidative phosphorylation and also with the increase of genes related to mitochondrial damage (Figure 2C,D).

Table 1. Top 25 Significantly Upregulated Mouse and Rat Genes in Differentiated F11 Cells Exposed to 10 μM Zalcitabine during Differentiation Quantified by RNA-seq[a]

mouse			rat		
position	expression (expr.) log ratio	symbol	position	expr. log ratio	symbol
1	2.09	*Taf7l*	1	2.05	*Sytl1*
2	1.81	*Nqo1*	2	2.00	*Kcnj3*
3	1.76	*Sytl1*	3	1.89	*Zbtb32*
4	1.64	*Ppef1*	4	1.86	*Galnt5*
5	1.52	*Ca6*	5	1.78	*Gsta1*
6	1.50	*Atp2a3*	6	1.75	*Wisp2*
7	1.50	*Gsdmd*	7	1.69	*Ppef1*
8	1.49	*Kcne5*	8	1.66	*Pimreg*
9	1.45	*Akr1b7*	9	1.54	*Pax4*
10	1.43	*4930481a15rik*	10	1.50	*Apobec2*
11	1.43	*Pax4*	11	1.50	*Akr1b10*
12	1.40	*Trim63*	12	1.49	*Mir-671*
13	1.40	*Spon2*	13	1.44	*Nqo1*
14	1.38	*Mir-671*	14	1.39	*Slc30a3*
15	1.37	*Clcf1*	15	1.38	*Spon2*
16	1.33	*Col13a1*	16	1.37	*Slc22a4*
17	1.32	*Chtf18*	17	1.36	*Atp2a3*
18	1.30	*Cpxm1*	18	1.34	*Trim63*
19	1.29	*Mt2*	19	1.32	*Apobr*
20	1.28	*Nppb*	20	1.32	*Ncf2*
21	1.26	*Pimreg*	21	1.31	*Col13a1*
22	1.24	*Kcp*	22	1.30	*Myh7b*
23	1.22	*Adgrf4*	23	1.30	*Nkx2−8*
24	1.22	*Lctl*	24	1.29	*Clcf1*
25	1.22	*Ccdc88b*	25	1.29	*Slc1a7*

[a]Data is the mean of three experiments with different samples.

To validate the effect of zalcitabine on the upregulation of genes related to oxidative stress, we compared the concentration of ROS in differentiated F11 cells exposed to zalcitabine during differentiation and in control differentiated F11 cells. We observed that zalcitabine increased the concentration of ROS in an 8.1%, leading to higher oxidative stress (Figure 3A−C) ($p < 0.05$, Student's t test). Despite the fact that this increase in ROS concentration is small, it was also observed in DRG neurons when they were exposed to other drugs that induce neuropathic pain like cisplatin.[18] Those expositions were enough to produce mitochondrial damage in neuronal cells.[19,20] The observed increase in ROS concentrations in differentiated F11 cells exposed to zalcitabine during differentiation has a translational relationship with DRG neurons in patients suffering from neuropathies induced by antiretroviral drugs due to damage in mitochondrial DNA, in which an increase in oxidative stress has been described.[21,22]

It has also been described that the increase in intracellular calcium concentration in animal models of neuropathic pain is strongly related to higher levels of ROS.[23,24] Previous studies pointed out that antiretroviral treatments elicited dramatic changes in the activity of voltage-gated calcium channels and in intracellular calcium concentrations.[25] In agreement with this, we observed that the exposure to zalcitabine during differentiation elicited an increase in the entrance of calcium in response to changes in membrane potential in differentiated F11 cells, but the treatment induced a decrease in SOCE (store-operated calcium entry) (Figure 3D,E) ($p < 0.05$, Student's t test). This demonstrates that the increase in calcium entry elicited by KCl is due to the entrance of calcium from the extracellular medium but not from endoplasmic reticulum stores and is in agreement with our previous study, in which we described the implication of voltage-gated calcium channels in neuropathic pain induced by an inflammatory stress in DRG neurons.[7] Furthermore, we observed that exposure to the antiretroviral lessens the transcription of genes encoding transient receptor potential canonical (TRPC) channels (Table S1, Figure S2) that are involved in SOCE.[26] These findings are in accordance with the results obtained by Staaf et al. (2009) in animal models of neuropathic pain, in which there was a reduction in the expression of TRPC channels, indicating that these channels modulate pain signaling.[27]

Among the genes related to oxidative stress and calcium signaling whose expression was increased in differentiated F11 cells after exposure to zalcitabine during differentiation, *Nqo1* and *Atp2a3* were upregulated (Figure 2E) ($p < 0.01$ for *Nqo1* and $p < 0.05$ for *Atp2a3*, Student's t test). *Nqo1* encodes NAD(P)H quinone dehydrogenase, an enzyme involved in the defense against both exogenous and endogenous quinones by the reduction of the substrate.[28] Although it has been proposed as an antitumor target, its role in pain is still controversial.[29,30]

The upregulation of *Atp2a3*, which encodes SERCA3 (a pump that takes calcium ions from the cytoplasm and introduces them into the endoplasmic reticulum, thus maintaining a constant cytosol Ca^{2+} concentration[31]), is in accordance with the fact that it has been described that zalcitabine led to an increase in the expression of genes encoding sarcoplasmic/endoplasmic reticulum calcium ATPases in animal models.[12] Nevertheless, the role of SERCA3 in pain has yet to be clearly established.

An increase in the expression of *Nqo1* and *Atp2a3* was also observed after exposition to F11 cells to a combination of inflammatory mediators composed by 10 μM histamine, 10 μM serotonin, 10 μM prostaglandin E_2, and 1 μM bradykinin (Figure S3; Table S3), suggesting that both genes are involved not only in iatrogenic neuropathic pain but also in neuropathic pain by an inflammatory origin.

To study the role of these genes in the zalcitabine-elicited increase in oxidative stress and calcium regulation, we evaluated the effect of the gain-of-function of those genes by overexpressing them independently. Overexpression of both *Nqo1* and *Atp2a3* elicited an increase in the intracellular concentration of calcium in response to KCl (Figure 4A,B) (p

https://doi.org/10.1021/acschemneuro.1c00129
ACS Chem. Neurosci. 2021, 12, 2619−2628

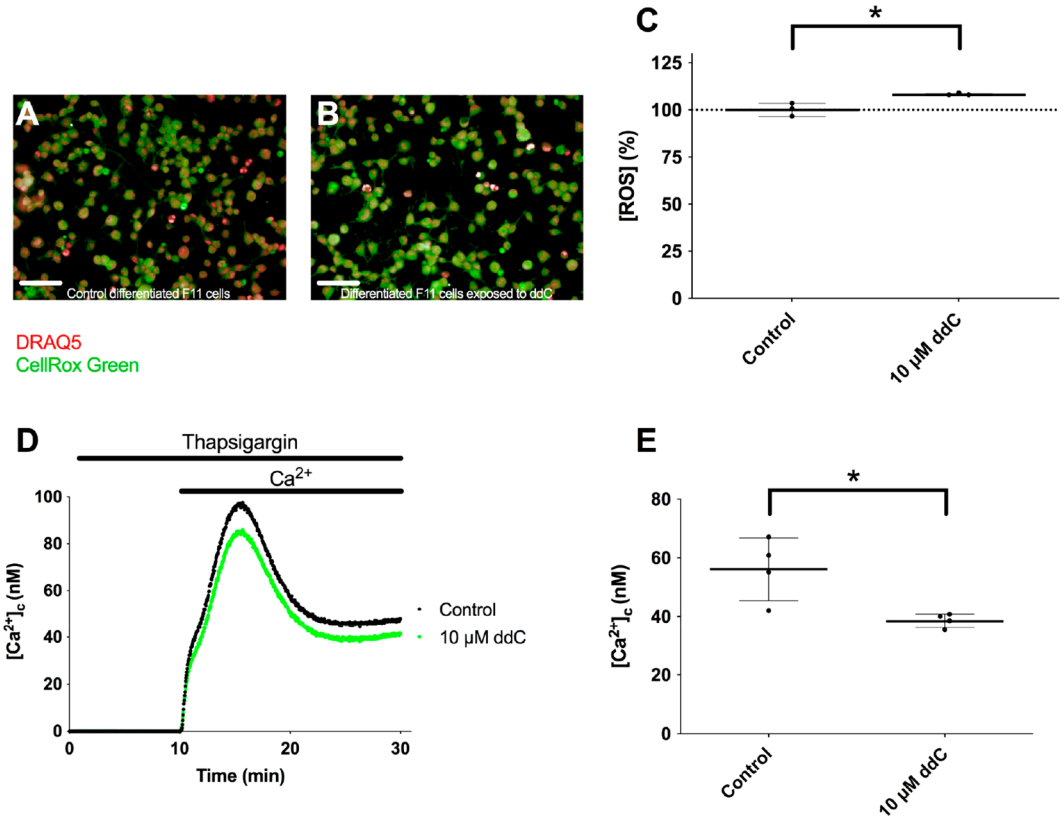

Figure 3. Exposure to zalcitabine during differentiation induces an increase in oxidative stress and a reduction in SOCE in differentiated F11 cells. Representative microphotographs of ROS accumulation stained with CellRox Green in (A) control differentiated F11 cells and (B) in differentiated F11 cells exposed to zalcitabine (ddC) during differentiation and (C) intracellular concentration of ROS measured by CellRox Green probe. Photographs are representative of three assays ($n = 3$) with 18 replicates per condition. Scale bar = 50 μm. Values shown for part C are means ± SD of three assays ($n = 3$) with 18 replicates per measurement. * $p < 0.05$ (Student's t test). (D) Calcium transients evoked by calcium restoration after exposure to 1 μM thapsigargin in differentiated F11 cells exposed and not exposed to zalcitabine (ddC) during differentiation and (E) summary of results of responses to calcium restoration 14 min after the addition of thapsigargin. Values shown for part D are means of one representative assay of four experiments with 24 replicates per measurement. Values shown for part E are means ± SD of four assays ($n = 4$) with 24 replicates per measurement. *$p < 0.05$ (Student's t test).

< 0.001 for *Nqo1*, $p < 0.01$ for *Atp2a3*, extra sum-of-squares F test), associated with a reduction in SOCE (Figure 4C,D) ($p < 0.05$, Student's t test), and also an increase in the intracellular oxidative stress (Figure 4E−H) ($p < 0.01$, Student's t test).

NAD(P)H quinone dehydrogenase is an enzyme usually related with protection against oxidative substances. However, it has been described in cells exposed to ozone or to naphthoquinones that NAD(P)H quinone dehydrogenase can also increase the production of ROS by the autoxidation of NAD(P)H quinone dehydrogenase derived products.[32,33] Interestingly, a reduction in SOCE is related with an increase in the expression of the NAD(P)H quinone dehydrogenase in murine embryonic fibroblasts lacking STIM1, an important regulator of SOCE for the adaption to cellular energy needs.[34]

The overexpression of *Atp2a3* induces an increase in the entrance of calcium into the endoplasmic reticulum. Because SOCE is a mechanism for the regulation of calcium concentration activated when endoplasmic reticulum calcium stores are empty,[35] when the entrance of calcium into these stores is enhanced, SOCE is stopped. The increase in the entrance into endoplasmic reticulum stores was accompanied by a compensatory entry of extracellular calcium into the cytoplasm and by an increase in the ROS concentration in differentiated F11 cells. This allows us to connect the changes observed in calcium homeostasis and the increase in oxidative stress elicited by zalcitabine in differentiated F11 cells with the effect of *Nqo1* and *Atp2a3* overexpression.

In summary, we have found how zalcitabine alters calcium signaling and oxidative phenotypic stress in immortalized DRG neurons, leading to cell hyperexcitability. Transient overexpression of *Nqo1* and *Atp2a3* genes encoding proteins involved in these two processes elicits an increase in oxidative stress and in the entrance of calcium from the extracellular medium into the cytoplasm, mimicking the effect of antiretroviral exposure on DRG neuronlike cells. These results demonstrate that the disbalance in intracellular calcium levels and the increase in ROS through the increase in the expression of these two genes are the molecular mechanisms of antiretroviral-induced damage in a model of DRG neurons. Despite the fact that those results may be confirmed in primary DRG neurons, they shed light on novel therapeutic targets for iatrogenic, antiretroviral-induced neuropathic pain.

METHODS

Reagents. KCl (131494; Panreac-AppliChem, Castellar del Vallès, Barcelona, Spain), $CaCl_2$ (22320.298; VWR, Llinars del Vallès, Barcelona, Spain), histamine (H7250; Sigma-Aldrich, Madrid, Spain), and serotonin (H9523; Sigma-Aldrich) were freshly weighed and dissolved before each assay. Zalcitabine (ddC; 16019; Cayman, Ann Arbor, MI, USA), prostaglandin E_2 (14010; Cayman), bradykinin (HY-P0206; Haoyuan Chemexpress, Shanghai, China), and thapsi-

https://doi.org/10.1021/acschemneuro.1c00129
ACS Chem. Neurosci. 2021, 12, 2619−2628

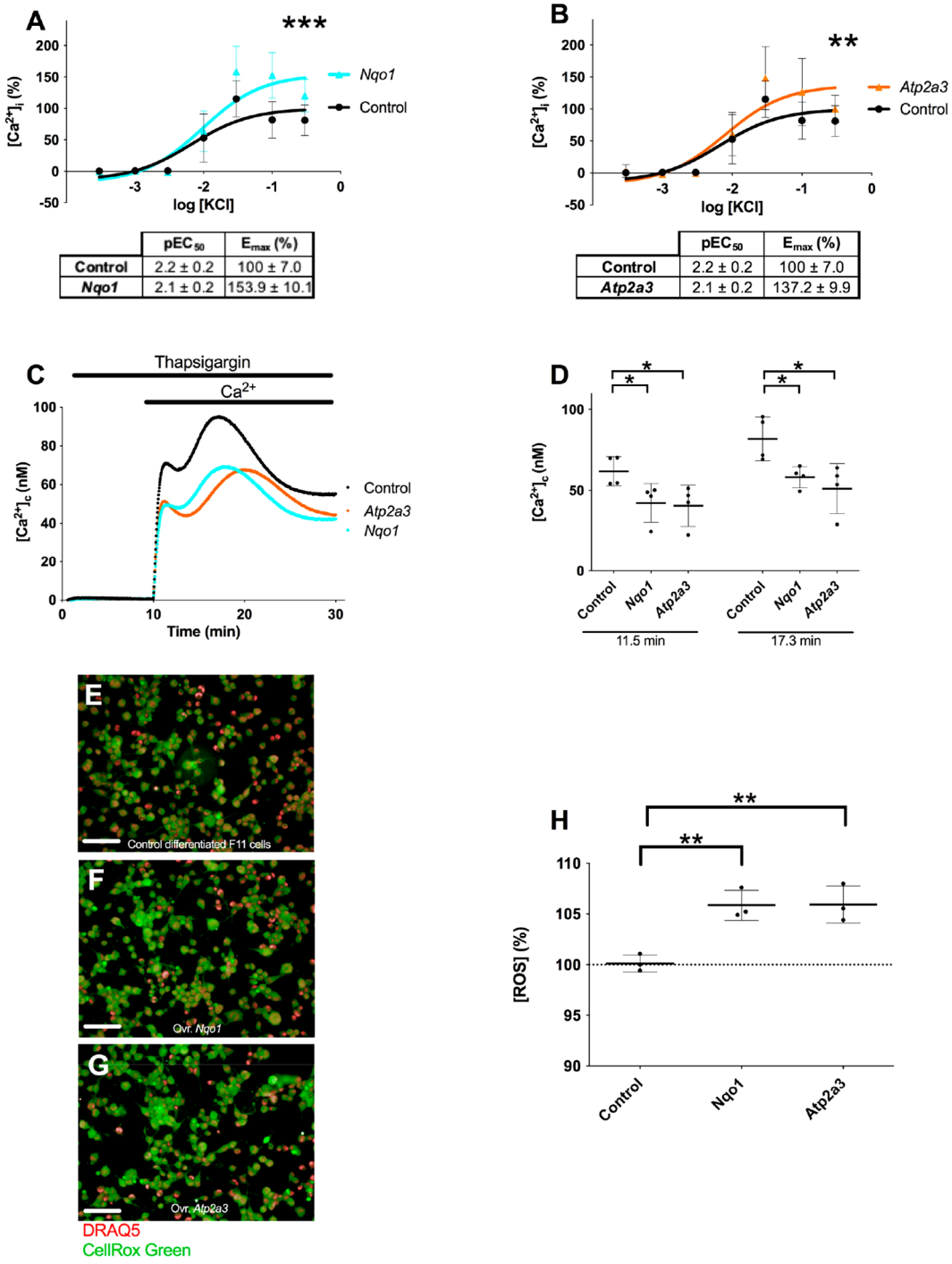

	pEC_{50}	E_{max} (%)
Control	2.2 ± 0.2	100 ± 7.0
Nqo1	2.1 ± 0.2	153.9 ± 10.1

	pEC_{50}	E_{max} (%)
Control	2.2 ± 0.2	100 ± 7.0
Atp2a3	2.1 ± 0.2	137.2 ± 9.9

Figure 4. Overexpression of *Nqo1* and *Atp2a3* denoted a key role of NAD(P)H quinone dehydrogenase and SERCA3 in zalcitabine-induced stress. Intracellular calcium mobilization elicited by KCl in (A) differentiated F11 cells in which *Nqo1* gene was overexpressed compared to control differentiated F11 cells and (B) differentiated F11 cells in which *Atp2a3* gene was overexpressed compared to control differentiated F11 cells. Values shown are means ± SD of four experiments ($n = 4$) with measurements in triplicate. ***$p < 0.001$; **$p < 0.01$ (extra sum-of-squares F test). (C) Calcium transients brought about by calcium restoration after exposition to 1 μM thapsigargin in control differentiated F11 cells and in differentiated F11 cells after overexpression of *Nqo1* and *Atp2a3* genes and (D) summary of results of responses to calcium restoration 11.5 and 17.3 min after the addition of thapsigargin in control differentiated F11 cells and in differentiated F11 cells after overexpression of *Nqo1* and *Atp2a3* genes. Values shown for part C are means of one representative assay of four experiments with 12 replicates per measurement. Values shown for part D are means ± SD of four assays ($n = 4$) with 12 replicates per measurement. * $p < 0.05$ (Student's t test). Representative microphotographs of ROS accumulation stained with CellRox Green in (E) control differentiated F11 cells and in differentiated F11 cells after transfection with (F) *Nqo1* and (G) *Atp2a3*. Photographs are representative of three assays ($n = 3$) with 16 replicates per condition. Scale bar = 50 μm. (H) Intracellular concentration of ROS measured by CellRox Green in differentiated F11 cells after overexpression of *Nqo1* and *Atp2a3* compared to control differentiated F11 cells. Values shown are means ± SD of three experiments ($n = 3$) with 16 replicates per measurement. ** $p < 0.01$ (Student's *t* test).

https://doi.org/10.1021/acschemneuro.1c00129
ACS Chem. Neurosci. 2021, 12, 2619−2628

gargin (T9033; Sigma-Aldrich) were diluted in DMSO (dimethyl sulfoxide; D8418; Sigma-Aldrich) at a stock concentration of 10 mM and stored at −20 °C.

Cell Culture and Differentiation. Mouse neuroblastoma/rat embryonic DRG neuron hybrid F11 cells (08062601; ECCAC, Salisbury, England, UK) were cultured in Dulbecco's Modified Eagle's Medium (DMEM) without sodium pyruvate (D5671; Sigma-Aldrich) supplemented with 10% (v/v) nondialyzed fetal calf serum (FBS; F9665; Sigma-Aldrich), 2 mM glutamine (G7513; Sigma-Aldrich), and 100 units/mL penicillin and 100 μg/mL streptomycin (P0781; Sigma-Aldrich) in a humidified atmosphere containing 5% carbon dioxide, at 37 °C. F11 cells were routinely checked for mycoplasma contamination and tested negative. Maximum number of passages was 22.

Differentiation was achieved by exposing F11 cells for 72 to a differentiation medium containing 1 mM dibutyryl-cAMP (N^6,2′-*O*-Dibutyryladenosine 3′,5′-cyclic monophosphate) (sc-201567; Santa Cruz Biotechnologies, Heidelberg; Germany), 30 μM forskolin (sc-3562; Santa Cruz Biotechnologies), 0.5% dialyzed fetal calf serum (F0392; Sigma-Aldrich), 100 units/mL penicillin, and 100 μg/mL streptomycin and 2 mM glutamine in DMEM without sodium pyruvate.

Measurement of Calcium Transients. F11 cells were seeded in clear, flat-bottomed, black-walled, 384-well plates (781091; Greiner Bio-One, Frickenhausen, Baden-Württemberg, Germany), pretreated with 2 μg/mL laminin (L2020; Sigma-Aldrich) and 30 μg/mL poly-D-lysine (P6407; Sigma-Aldrich) at a density of 5000 cells/well. After 24 h, culture medium was replaced by 10 μM zalcitabine diluted in differentiation medium in the corresponding wells. After 72 h, the medium was removed and replaced by 25 μL of fresh medium and incubatedwith 25 μL of FLIPR Calcium-6 dye (R8190; Molecular Devices, Sunnyvale, CA), diluted in HBSS containing 20 mM HEPES [(4-(2-hydroxyethyl)-1-piperazineethanesulfonic acid); H3375; Sigma-Aldrich] (pH 7.4), for 2 h at 37 °C. Changes in intracellular calcium concentration ($[Ca^{2+}]_i$) were recorded with a FDSS7000EX Functional Drug Screen System (Hamamatsu Photonics, Cerdanyola del Vallès, Barcelona, Spain) by excitation of the calcium-sensitive fluorescent dye with a light source at 470−495 nm and emission in the 515−575 nm range. FDSS tips (A8687-62; Hamamatsu Photonics) were pretreated with a solution of 0.1% BSA (Bovine Serum Albumin; 10775835001; Sigma-Aldrich) diluted in the assay buffer. $[Ca^{2+}]_i$ responses were obtained as the difference between the maximum and the minimum fluorescence values by considering the peak elicited by KCl. Four independent sets of experiments, each with three replicates, were performed. Data was normalized to the maximum response to KCl of differentiated cells.

Store-operated calcium entry (SOCE) measurements were performed as previously described.[35] Briefly, F11 cells were seeded, differentiated, and transfected as exposed. FLIPR Calcium-6 dye was dissolved in calcium-free HBSS (HEPES-buffered saline), in which Ca^{2+} was omitted, and 1 mM BAPTA [1,2-bis(o-aminophenoxy) ethane-*N*,*N*,*N*′,*N*′-tetraacetic acid; A4926; Sigma-Aldrich] was added. After being incubated for 2 h at 37 °C, fluorescence was measured in a FDSS7000EX Functional Drug Screen System as exposed. Fluorescence was calibrated to calcium concentration ($[Ca^{2+}]$) using the following formula:

$$[Ca^{2+}] = K_D \times \left(\frac{F - F_{min}}{F_{max} - F}\right)$$

where K_D = 320 nM, F is the measured fluorescence, F_{max} is the fluorescence value determined after addition of 0.1% Triton X-100 (101556683; Sigma-Aldrich) with 10 mM $CaCl_2$ in HBSS, and F_{min} is the fluorescence value determined after addition of 0.1% Triton X-100 with 10 mM BAPTA in HBSS. At least three independent sets of experiments were performed, each with 12 replicates.

Measurement of Oxidative Stress. F11 cells were seeded in clear, flat-bottomed, black-walled, 384-well plates pretreated with 30 μg/mL poly-D-lysine at a density of 2500 cells/well. After 24 h, culture medium was replaced by differentiation medium containing 10 μM zalcitabine in the corresponding wells. After 72 h, CellRox Green (C10444; Thermo Fisher Scientific) was added to a final concentration of 5 μM. Thirty minutes later, the F11 cells were fixed for 15 min with 4% paraformaldehyde (158127; Sigma-Aldrich) in FBS at 4 °C and were stained with 1.5 μg/mL wheat germ agglutinin conjugated with Alexa Fluor 555 (W32464; Invitrogen, Paisley, UK) and 2.5 μM nuclear stain DRAQ5 (108410; Abcam, Cambridge, UK). An Operetta High-Content Imaging System (PerkinElmer, Tres Cantos, Madrid, Spain) was used to capture fluorescence and bright field images (5 fields per well, 20x). Image analysis was conducted using the Harmony High Content Imaging and Analysis Software (PerkinElmer), considering the mean intensity of green fluorescence in the cytoplasm of F11 cells only. To do this, we programmed the software to measure only the intensity of the dye in the cytoplasm, surrounded by the cell membrane, which was stained with the wheat germ agglutinin conjugated with Alexa Fluor 555. Three independent sets of experiments, each with 18 replicates, were performed.

Microscopy Assays. Cells were plated on clear-bottom 96-well plates (6005558; PerkinElmer) previously treated with 30 μg/mL poly-D-lysine. Cells were seeded in 50 μL of culture medium at a density of 7500 per well. After 24 h, the culture medium was replaced by differentiation medium containing 10 μM zalcitabine in the corresponding wells. At 72 h after medium replacement, F11 cells were fixed for 20 min with 4% paraformaldehyde in PBS at 4 °C. The cells were then washed twice with HBSS before being permeabilized with blocking buffer containing 5% BSA and 0.1% Triton X-100 (T8787; Sigma-Aldrich) in HBSS for 30 min at room temperature. The cells were then stained for 1 h with a 1:500 dilution of Alexa 488 dye-conjugated anti-ß-tubulin mouse antibody (558605; Becton & Dickinson Biosciences, San Agustín de Guadalix, Madrid, Spain), as a neuron-specific marker,[36] and 2.5 μM nuclear stain DRAQ5. An Operetta High-Content Imaging System (PerkinElmer, Tres Cantos, Madrid, Spain) was used to capture all fluorescence and bright field images (12 fields per well, 20x). Image analysis was conducted with the Harmony High Content Imaging and Analysis Software considering maximum neurite length in each well. Three independent sets of experiments, each with 16 replicates, were performed. Results were normalized to the maximum neurite length of differentiated cells.

The analysis of the number of connections between cells was performed after staining cells employing the exposed protocol. An Operetta High-Content Imaging System was employed to capture all fluorescence and bright field images (9 fields per well, 10x). Image analysis was conducted with the Harmony High Content Imaging and Analysis Software considering the number of nodes, the maximum neurite length, and the mean neurite length in each well.

RNA Sequencing. F11 cells were seeded in Corning square bioassay dishes (CLS43110; Sigma-Aldrich) at a concentration of 20 million cells per dish and differentiated 24 h later. After 72 h, cells were exposed to 10 μM zalcitabine or to a combination of inflammatory mediators composed by 10 μM histamine, 10 μM serotonin, 10 μM prostaglandin E2, and 1 μM bradykinin. Total RNA from F11 cells was extracted and purified with the RNeasy Mini Kit (Qiagen, Hilden, Germany). RNA quantity, integrity, and quality were estimated employing a 2100 Agilent Bioanalyzer (Agilent Technologies, Las Rozas, Madrid, Spain) to calculate RIN (RNA integrity number). All the samples had RIN values greater than 8. Sequencing was performed using the NextSeq 500 platform (Illumina, San Diego, CA, USA). Three RNaseq experiments were performed with independent samples.

Bioinformatics Analysis of RNA-seq Data. Reads were individually mapped against both the mouse genome assembly NCBI37/mm9 and the rat genome RGSC Rnor_5.0/rn5. First, the quality of the generated data was tested, using FastQC and Prinseq (Babraham Bioinformatics, Cambridge, UK). The 440 M high quality reads were obtained (91% of total reads). Subsequently, duplicated sequences were detected using Picard tools (Picard tools, Cambridge, MA, USA) and aligned with the specific gene sequence by the STAR algorithm (Spliced Transcripts Alignment to a Reference). A quality control of generated data was performed with RNA-SeQC. The

https://doi.org/10.1021/acschemneuro.1c00129
ACS Chem. Neurosci. 2021, 12, 2619−2628

quantification of the expression of each gene was performed using the HOMER (Hypergeometric Optimization of Motif EnRichment) software, performing the differential gene expression analysis by R tools.[37] Differential expression analysis was performed using the *edgeR* R package.[38] Sequences were previously filtered by selecting only genes present in at least 3 samples with a count value greater than 1 cpm. Multidimensional scaling was also performed, to explore the overall differences between groups. A quasi-likelihood F test was used to test for differential expression, using a negative binomial generalized linear model. Afterward, the top differential expressed genes (FDR adjusted p-value <0.05) were employed to perform a biological interpretation analysis of the differential expression between categories, using the IPA (Ingenuity Pathway Analysis) software (Quiagen).

Real Time Reverse Polymerase Chain Reaction (RT-qPCR). RNA for RT-qPCR was obtained employing the same methodology as RNA for RNA sequencing. RT-qPCR was performed with 5 ng of RNA, using the EXPRESS One-Step Superscript qRT-PCR kit (11781200; Thermo Fisher Scientific, Alcobendas, Madrid, Spain). Gene expression was determined through TaqMan assays on a QuantStudio 12K Flex reader (Life Technologies, Carlsbad, CA, USA). Gene-specific probes and primers from Applied Biosystems (Foster City, CA, USA) were used. Two TaqMan gene expression assays were employed: *Nqo1* (Rn00566528_m1) and *Atp2a3* (Rn00563800_m1). All templates were analyzed in triplicate, and the quantification cycle (C_q) value of each gene was normalized to *36b4*, according to $\Delta C_q = C_q$ (examined gene) $- C_q$ (*36b4*). The relative amount of each mRNA after exposition to each drug was normalized to the expression of the gene in control differentiated F11 cells and transformed in a fold change in arbitrary unit (AU) values using the equation $AU = 2^{-\Delta\Delta C_q}$.

Plasmid Transfection. *Nqo1* plasmid was a gift from Yosef Shaul (Addgene plasmid no. 61735; http://n2t.net/addgene:61735; RRID: Addgene_61735).[39] *Atp2a3* plasmid was a gift from Jonathan Lytton & David MacLennan (Addgene plasmid no. 75189; http://n2t.net/addgene:75189; RRID:Addgene_75189).[40] pcDNA3 empty vector was a gift from Marian Castro. Plasmids were purified with Nucleobond Xtra Midi EF Kit (740420; Macherey-Nagel GmBH, Düren; Germany).

Reverse transfection was performed with 0.0768 μg of DNA and 0.3072 μL of FuGENE HD (E2312; Promega Biotech, Alcobendas, Madrid, Spain) per well (ratio 1:4). Cells were seeded and transfected in clear, flat-bottomed, black-walled, 384-well plates at a density of 2500 cells per well in culture medium; 72 h later, the culture medium was substituted by the differentiation medium. Transfection efficiency was confirmed by parallel transfection, with a construct coding for GFP protein, and overexpression was tested by RT-qPCR, seeding, and transfecting 10^5 F11 cells per well in 12-well, clear, flat-bottomed, TC-treated multiwell cell culture plates (353043; Corning, Tewksbury, MA, USA).

Data Analysis. Data analysis was performed using GraphPad Prism 6.0 software (GraphPad Software, La Jolla, CA). A sigmoidal dose−response model was used to fit the concentration−response curves. The data fits were compared using the extra sum-of-squares F test. Neurite length assays, oxidative stress, SOCE quantification, and RT-qPCR data were compared by Student's t test for statistic hypothesis inference. Differences were considered statistically significant at $p < 0.05$.

■ ASSOCIATED CONTENT

Supporting Information

The Supporting Information is available free of charge at https://pubs.acs.org/doi/10.1021/acschemneuro.1c00129.

Study of effect of ddC on neurite length and on connectivity between differentiated F11 cells, characterization of the expression of genes encoding proteins related to SOCE in differentiated F11 cells exposed to 10 μM ddC, and effect on transcriptome of exposition to a combination of inflammatory mediators in differentiating F11 cells (PDF)

■ AUTHOR INFORMATION

Corresponding Authors

Javier Burgueño − *WeLab Barcelona, Parc Científic de Barcelona, 08028 Barcelona, Spain*; Email: jburgueno@welab.barcelona

María I. Loza − *BioFarma Research Group, Centro Singular de Investigación en Medicina Molecular y Enfermedades Crónicas (CIMUS), Universidade de Santiago de Compostela, 15782 Santiago de Compostela, Spain*; orcid.org/0000-0003-4730-0863; Email: mabel.loza@usc.es

Authors

Antón L. Martínez − *BioFarma Research Group, Centro Singular de Investigación en Medicina Molecular y Enfermedades Crónicas (CIMUS), Universidade de Santiago de Compostela, 15782 Santiago de Compostela, Spain*; orcid.org/0000-0002-1595-3459

José Brea − *BioFarma Research Group, Centro Singular de Investigación en Medicina Molecular y Enfermedades Crónicas (CIMUS), Universidade de Santiago de Compostela, 15782 Santiago de Compostela, Spain*

Eduardo Domínguez − *BioFarma Research Group, Centro Singular de Investigación en Medicina Molecular y Enfermedades Crónicas (CIMUS), Universidade de Santiago de Compostela, 15782 Santiago de Compostela, Spain*

María J. Varela − *BioFarma Research Group, Centro Singular de Investigación en Medicina Molecular y Enfermedades Crónicas (CIMUS), Universidade de Santiago de Compostela, 15782 Santiago de Compostela, Spain*

Marta Cimadevila − *BioFarma Research Group, Centro Singular de Investigación en Medicina Molecular y Enfermedades Crónicas (CIMUS), Universidade de Santiago de Compostela, 15782 Santiago de Compostela, Spain*; orcid.org/0000-0002-5090-8311

Catarina Allegue − *Grupo de Medicina Xenómica, CIBERER, Universidade de Santiago de Compostela, 15782 Santiago de Compostela, Spain*

Raquel Cruz − *Grupo de Medicina Xenómica, CIBERER, Universidade de Santiago de Compostela, 15782 Santiago de Compostela, Spain*

Xavier Monroy − *WeLab Barcelona, Parc Científic de Barcelona, 08028 Barcelona, Spain*

Manuel Merlos − *WeLab Barcelona, Parc Científic de Barcelona, 08028 Barcelona, Spain*

Ángel Carracedo − *Grupo de Medicina Xenómica, CIBERER, Universidade de Santiago de Compostela, 15782 Santiago de Compostela, Spain; Fundación Pública Galega de Medicina Xenómica, IDIS, SERGAS, 15706 Santiago de Compostela, Spain*

Complete contact information is available at: https://pubs.acs.org/10.1021/acschemneuro.1c00129

Author Contributions

$^{\perp}$A.L.M. and J.O.B. contributed equally to this work. M.I.L., J.O.B. and E.D. were involved in planning and supervising the work. A.L.M., M.C., and M.J.V. performed the experiments. C.A. and R.C. performed the analysis of RNA-seq. A.L.M. and M.J.V. processed and analyzed the experimental data. M.I.L.,

https://doi.org/10.1021/acschemneuro.1c00129
ACS Chem. Neurosci. 2021, 12, 2619−2628

E.D., and J.O.B. drafted the manuscript and designed the figures. A.C., J.A.B., X.M., and M.M. aided in interpreting the results. All authors discussed the results and commented on the manuscript.

Funding

This work was supported by the Joint R&D Unit Esteve-USC (IN853A-2017/6), cofinanced by the Galician Innovation Agency and the Spanish Ministry of Economy and Competitiveness (MINECO) within the framework of the Spanish Strategy of Innovation in Galicia, and by the Phenopain project (RTC-2015-4207-1) of the RETOS-COLABORACIÓN program of the MINECO, cofinanced by the European Union through the European Regional Development Fund (ERDF). A.L.M. was in receipt of a predoctoral fellowship from the FPU program (Spanish Ministry of Education, Culture and Sports).

Notes

The authors declare the following competing financial interest(s): WeLab Barcelona provided support in the form of salaries for X.M., M.M., and J.A.B. but did not have any additional role in the study design, data collection and analysis, decision to publish, or preparation of the manuscript. The specific roles of these authors are articulated in the Author Contributions section.

■ ABBREVIATIONS

AMP, adenosine monophosphate; ATP, adenosine triphosphate; BAPTA, 1,2-bis(o-aminophenoxy) ethane-*N*,*N*,*N*′,*N*′-tetraacetic acid; BSA, bovine serum albumin; ddC, zalcitabine; DMEM, Dulbecco's modified Eagle's medium; DMSO, dimethyl sulfoxide; DNA, deoxyribonucleic acid; DRG, dorsal root ganglia; HBSS, Hank's balanced salt solution; HEPES, 4-(2-hydroxyethyl)-1-piperazineethanesulfonic acid; HIV, human immunodeficiency virus; NAD(P)H, nicotinamide adenine dinucleotide phosphate; PBS, phosphate buffer solution; RIN, RNA integrity number; RNA, ribonucleic acid; ROS, reactive oxygen species; RT-qPCR, reverse transcription quantitative polymerase chain reaction; SERCA3, sarcoplasmic/endoplasmic reticulum calcium ATPase 3; SOCE, store-operated calcium entry; TRPC, transient receptor potential canonical

■ REFERENCES

(1) Jensen, T. S., and Finnerup, N. B. (2014) Allodynia and Hyperalgesia in Neuropathic Pain: Clinical Manifestations and Mechanisms. *Lancet Neurol. 13* (9), 924−935.

(2) Brandolini, L., Benedetti, E., Ruffini, P. A., Russo, R., Cristiano, L., Antonosante, A., D'Angelo, M., Castelli, V., Giordano, A., Allegretti, M., et al. (2017) CXCR1/2 Pathways in Paclitaxel-Induced Neuropathic Pain. *Oncotarget 8* (14), 23188−23201.

(3) Poorolajal, J., Hooshmand, E., Mahjub, H., Esmailnasab, N., and Jenabi, E. (2016) Survival Rate of AIDS Disease and Mortality in HIV-Infected Patients: A Meta-Analysis. *Public Health 139*, 3−12.

(4) Adkins, J. C., Peters, D. H., and Faulds, D. (1997) Zalcitabine: An Update of Its Pharmacodynamic and Pharmacokinetic Properties and Clinical Efficacy in the Management of HIV Infection. *Drugs 53* (6), 1054−1080.

(5) Alles, S. R. A., and Smith, P. A. (2018) Etiology and Pharmacology of Neuropathic Pain. *Pharmacol. Rev. 70* (2), 315−347.

(6) Doran, C., Chetrit, J., Holley, M. C., Grundy, D., and Nassar, M. A. (2015) Mouse DRG Cell Line with Properties of Nociceptors. *PLoS One 10* (6), No. e0128670.

(7) Martínez, A. L., Brea, J., Monroy, X., Merlos, M., Burgueño, J., and Loza, M. I. (2019) A New Model of Sensorial Neuron-Like Cells for HTS of Novel Analgesics for Neuropathic Pain. *SLAS Discovery 24* (2), 158−168.

(8) Haberberger, R. V., Barry, C., and Matusica, D. (2020) Immortalized Dorsal Root Ganglion Neuron Cell Lines. *Front. Cell. Neurosci. 14* (June), 1 DOI: 10.3389/fncel.2020.00184.

(9) Pastori, V., D'Aloia, A., Blasa, S., and Lecchi, M. (2019) Serum-Deprived Differentiated Neuroblastoma F-11 Cells Express Functional Dorsal Root Ganglion Neuron Properties. *PeerJ 2019* (10), 1−20.

(10) Yin, K., Baillie, G. J., and Vetter, I. (2016) Neuronal Cell Lines as Model Dorsal Root Ganglion Neurons: A Transcriptomic Comparison. *Mol. Pain 12*, 1−17.

(11) de Anda-Jáuregui, G., McGregor, B. A., Guo, K., and Hur, J. (2019) A Network Pharmacology Approach for the Identification of Common Mechanisms of Drug-Induced Peripheral Neuropathy. *CPT: Pharmacometrics Syst. Pharmacol. 8* (4), 211−219.

(12) Maratou, K., Wallace, V. C. J., Hasnie, F. S., Okuse, K., Hosseini, R., Jina, N., Blackbeard, J., Pheby, T., Orengo, C., Dickenson, A. H., et al. (2009) Comparison of Dorsal Root Ganglion Gene Expression in Rat Models of Traumatic and HIV-Associated Neuropathic Pain. *Eur. J. Pain 13* (4), 387−398.

(13) Jarvis, M. F., Scott, V. E., McGaraughty, S., Chu, K. L., Xu, J., Niforatos, W., Milicic, I., Joshi, S., Zhang, Q., and Xia, Z. (2014) A Peripherally Acting, Selective T-Type Calcium Channel Blocker, ABT-639, Effectively Reduces Nociceptive and Neuropathic Pain in Rats. *Biochem. Pharmacol. 89* (4), 536−544.

(14) Sanna, M. D., Stark, H., Lucarini, L., Ghelardini, C., Masini, E., and Galeotti, N. (2015) Histamine H4 Receptor Activation Alleviates Neuropathic Pain through Differential Regulation of ERK, JNK, and P38 MAPK Phosphorylation. *Pain 156* (12), 2492−2504.

(15) Martínez, A. L., Brea, J., Barro, M., Monroy, X., Merlos, M., Burgueño, J., and Loza, M. I. (2021) Development of a Novel in Vitro Assay to Screen for Neuroprotective Drugs against Iatrogenic Neurite Shortening. *PLoS One 16* (3), No. e0248139.

(16) De Clercq, E. (2005) Emerging Anti-HIV Drugs. *Expert Opin. Emerging Drugs 10* (2), 241−274.

(17) Hinckley, S., Sherman, S., Best, B. M., Momper, J., Ma, Q., Letendre, S. R., Ellis, R., and Bang, A. (2016) Neurotoxicity Screening of Antiretroviral Drugs with Human IPSC-Derived Neurons. In *Conference on Retroviruses and Opportunistic Infections*, Boston, MA.

(18) Leo, M., Schmitt, L. I., Küsterarent, P., Kutritz, A., Rassaf, T., Kleinschnitz, C., Hendgen-Cotta, U. B., and Hagenacker, T. (2020) Platinum-Based Drugs Cause Mitochondrial Dysfunction in Cultured Dorsal Root Ganglion Neurons. *Int. J. Mol. Sci. 21* (22), 1−8.

(19) Andres, A. L., Gong, X., Di, K., and Bota, D. A. (2014) Low-Doses of Cisplatin Injure Hippocampal Synapses: A Mechanism for 'Chemo' Brain? *Exp. Neurol. 255* (1), 137−144.

(20) Boukelmoune, N., Chiu, G. S., Kavelaars, A., and Heijnen, C. J. (2018) Mitochondrial Transfer from Mesenchymal Stem Cells to Neural Stem Cells Protects against the Neurotoxic Effects of Cisplatin. *Acta Neuropathol. Commun. 6* (1), 139.

(21) Iida, T., Yi, H., Liu, S., Huang, W., Kanda, H., Lubarsky, D. A., and Hao, S. (2016) Spinal CPEB-MtROS-CBP Signaling Pathway Contributes to Perineural HIV Gp120 with DdC-Related Neuropathic Pain in Rats. *Exp. Neurol. 281*, 17−27.

(22) Dalakas, M. C. (2001) Peripheral Neuropathy and Antiretroviral Drugs. *J. Peripher. Nerv. Syst. 6* (1), 14−20.

(23) Amin, B., Hajhashemi, V., Abnous, K., and Hosseinzadeh, H. (2014) Ceftriaxone, a Beta-Lactam Antibiotic, Modulates Apoptosis Pathways and Oxidative Stress in a Rat Model of Neuropathic Pain. *BioMed Res. Int. 2014*, 2014.

(24) Pathak, N. N., Balaganur, V., Lingaraju, M. C., Kant, V., Latief, N., More, A. S., Kumar, D., Kumar, D., and Tandan, S. K. (2014) Atorvastatin Attenuates Neuropathic Pain in Rat Neuropathy Model by Down-Regulating Oxidative Damage at Peripheral, Spinal and Supraspinal Levels. *Neurochem. Int. 68* (1), 1−9.

(25) Guo, Y., Zhang, Z., Wu, H., Luo, Z. D., Hogan, Q. H., and Pan, B. (2017) Increased Thrombospondin-4 after Nerve Injury Mediates

Disruption of Intracellular Calcium Signaling in Primary Sensory Neurons. *Neuropharmacology 117*, 292−304.
(26) Lopez, J. J., Jardin, I., Sanchez-Collado, J., Salido, G. M., Smani, T., and Rosado, J. A. (2020) TRPC Channels in the SOCE Scenario. *Cells 9* (1), 126.
(27) Staaf, S., Oerther, S., Lucas, G., Mattsson, J. P., and Ernfors, P. (2009) Differential Regulation of TRP Channels in a Rat Model of Neuropathic Pain. *Pain 144* (1−2), 187−199.
(28) Luo, S., Lei, K., Xiang, D., and Ye, K. (2018) NQO1 Is Regulated by PTEN in Glioblastoma, Mediating Cell Proliferation and Oxidative Stress. *Oxid. Med. Cell. Longevity 2018*, 2018.
(29) Megarity, C. F., Abdel-Aal Bettley, H., Caraher, M. C., Scott, K. A., Whitehead, R. C., Jowitt, T. A., Gutierrez, A., Bryce, R. A., Nolan, K. A., Stratford, I. J., Timson, D. J., et al. (2019) Negative Cooperativity in NAD(P)H Quinone Oxidoreductase 1 (NQO1). *ChemBioChem 20*, 1.
(30) Kadela-Tomanek, M., Bębenek, E., Chrobak, E., Marciniec, K., Latocha, M., Kuśmierz, D., Jastrzębska, M., and Boryczka, S. (2019) Betulin-1,4-Quinone Hybrids: Synthesis, Anticancer Activity and Molecular Docking Study with NQO1 Enzyme. *Eur. J. Med. Chem. 177*, 302−315.
(31) Elaïb, Z., Lopez, J. J., Coupaye, M., Zuber, K., Becker, Y., Kondratieff, A., Repérant, C., Pépin, M., Salomon, L., Teillet, F., et al. (2019) Platelet Functions Are Decreased in Obesity and Restored after Weight Loss: Evidence for a Role of the SERCA3-Dependent ADP Secretion Pathway. *Thromb. Haemostasis 119* (3), 384−396.
(32) Watanabe, N., and Forman, H. J. (2003) Autoxidation of Extracellular Hydroquinones Is a Causative Event for the Cytotoxicity of Menadione and DMNQ in A549-S Cells. *Arch. Biochem. Biophys. 411* (1), 145−157.
(33) Voynow, J. A., Fischer, B. M., Zheng, S., Potts, E. N., Grover, A. R., Jaiswal, A. K., Ghio, A. J., and Foster, W. M. (2009) NAD(P)H Quinone Oxidoreductase 1 Is Essential for Ozone-Induced Oxidative Stress in Mice and Humans. *Am. J. Respir. Cell Mol. Biol. 41* (1), 107−113.
(34) Henke, N., Albrecht, P., Pfeiffer, A., Toutzaris, D., Zanger, K., and Methner, A. (2012) Stromal Interaction Molecule 1 (STIM1) Is Involved in the Regulation of Mitochondrial Shape and Bioenergetics and Plays a Role in Oxidative Stress. *J. Biol. Chem. 287* (50), 42042−42052.
(35) Srivats, S., Balasuriya, D., Pasche, M., Vistal, G., Edwardson, J. M., Taylor, C. W., and Murrell-Lagnado, R. D. (2016) Sigma1 Receptors Inhibit Store-Operated Ca2+ Entry by Attenuating Coupling of STIM1 to Orai1. *J. Cell Biol. 213* (1), 65−79.
(36) Bhattacherjee, A., Liao, Z., and Smith, P. G. (2014) Trophic Factor and Hormonal Regulation of Neurite Outgrowth in Sensory Neuron-like 50B11 Cells. *Neurosci. Lett. 558*, 120−125.
(37) Heinz, S., Benner, C., Spann, N., Bertolino, E., Lin, Y. C., Laslo, P., Cheng, J. X., Murre, C., Singh, H., and Glass, C. K. (2010) Simple Combinations of Lineage-Determining Transcription Factors Prime Cis-Regulatory Elements Required for Macrophage and B Cell Identities. *Mol. Cell 38* (4), 576−589.
(38) Robinson, M. D., McCarthy, D. J., and Smyth, G. K. (2010) EdgeR: A Bioconductor Package for Differential Expression Analysis of Digital Gene Expression Data. *Bioinformatics 26* (1), 139−140.
(39) Asher, G., Tsvetkov, P., Kahana, C., and Shaul, Y. (2005) A Mechanism of Ubiquitin-Independent Proteasomal Degradation of the Tumor Suppressors P53 and P73. *Genes Dev. 19* (3), 316−321.
(40) Poch, E., Leach, S., Snape, S., Cacic, T., MacLennan, D. H., and Lytton, J. (1998) Functional Characterization of Alternatively Spliced Human SERCA3 Transcripts. *Am. J. Physiol. 275* (6), C1449−58.

https://doi.org/10.1021/acschemneuro.1c00129
ACS Chem. Neurosci. 2021, 12, 2619−2628